ACS APPLIED MATERIALS & INTERFACES

Research Article

www.acsami.org

Effect of Aging and PCBM Content on Bulk Heterojunction Organic Solar Cells Studied by Intensity Modulated Photocurrent Spectroscopy

Joshua C. Byers,[†] Thomas Heiser,[‡] Maksim Skorobogatiy,[§] and Oleg A. Semenikhin*[,†]

[†]Department of Chemistry, The University of Western Ontario, 1151 Richmond St., London, Ontario N6A 5B7, Canada

[‡]Institut d'Electronique du Solide et des Systèmes, Université de Strasbourg-CNRS, 23 rue du Loess, 67037 Strasbourg, France

[§]Génie Physique, École Polytechnique de Montréal, C.P. 6079, succ. Centre-ville, Montréal, Québec H3C 3A7, Canada

Supporting Information

ABSTRACT: A series of encapsulated and nonencapsulated bulk heterojunction photovoltaic devices containing poly(3-hexylthiophene) (P3HT) and [6,6]-phenyl C_{61} butyric acid methyl ester (PCBM) with different P3HT:PCBM ratios were investigated using traditional steady-state as well as non-steady-state intensity modulated photocurrent spectroscopy (IMPS) techniques. The steady state $J-V$ measurements showed that PCBM content did not have a significant effect on the efficiency for freshly prepared devices, whereas aged nonencapsulated devices exhibited a strong dependence on PCBM content. IMPS measurements showed a significant contribution of interfacial nongeminate recombination in nonencapsulated devices, which increased with decreasing PCBM content in the photoactive layer and cell aging. It was related to the formation of interfacial states at the P3HT/PCBM interface due to atmospheric contamination, which act as recombination centers. Device encapsulation was found to be effective in preventing the occurrence of interfacial recombination. Our results suggest that IMPS can be used as a diagnostic tool to predict the performance of bulk heterojunction organic solar cells. If a solar cell shows the presence of interfacial states as indicated by semicircle arcs in quadrant I of the IMPS complex plane plots, it is most likely that its performance will deteriorate with time due to enhanced interfacial recombination, even without further exposure to atmospheric contaminations. We conclude that interfacial nongeminate recombination is an important degradation mechanism in organic solar cells, especially in the case of exposure to atmospheric contaminants.

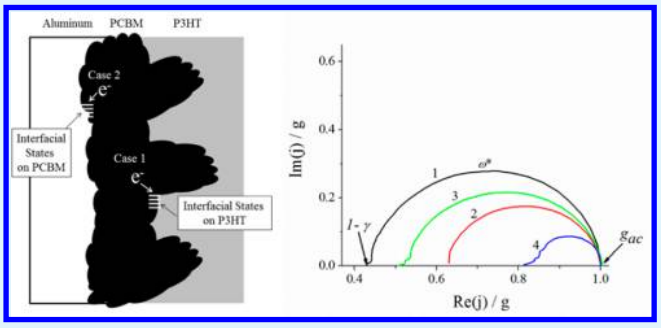

KEYWORDS: *organic photovoltaics, intensity modulated photocurrent spectroscopy (IMPS), intensity modulated photovoltage spectroscopy (IMVS), exciton, degradation, nongeminate recombination*

1. INTRODUCTION

Bulk heterojunction organic solar cells incorporating conjugated polymers and fullerene derivatives as a composite photoactive layer represent a promising platform for high-throughput, low cost alternative energy generation. Organic photovoltaic devices require the use of two materials in the photoactive layer due to the formation of excitons, instead of free charge carriers, upon light absorption in the conjugated polymer. Because of the short lifetimes of excitons, it is necessary to form an intimately mixed three-dimensional bulk heterojunction of the two materials to maximize the interfacial area while ensuring the formation of uninterrupted pathways for charge carriers to be transported across the film. However, even then, a significant fraction of photogenerated carriers is lost due to recombination. Generally, two recombination mechanisms are considered: geminate recombination, whereby both recombining carriers are generated simultaneously and form a primary exciton, and nongeminate recombination, which involves an electron and a hole that were photogenerated in separate acts and possibly quite far from each other. In the latter case, the recombination is often assisted by interfacial states, which can be envisioned as local states or traps that are located at an interface between two phases (e.g., PCBM and P3HT or PCMB or P3HT and metal contact, etc.) and can be accessed by both photogenerated electrons and holes. In recent years, nongeminate recombination has emerged as an important pathway of recombination losses in organic bulk heterojunction solar cells.[1−3] However, the mechanism of the recombination process and especially the origin of the interfacial states where nongeminate recombination occurs have yet to be clarified in sufficient detail.

One of the ongoing issues that limit the application of organic solar cells is the degradation of device performance during their lifetime.[4] Device efficiency has been shown to

Received: September 28, 2016
Accepted: October 5, 2016

DOI: 10.1021/acsami.6b12345
ACS Appl. Mater. Interfaces XXXX, XXX, XXX−XXX

decrease with time, especially under illumination, and this detrimental effect is further accelerated when the cells are operated in ambient conditions.[5−11] Practical devices will require a sustained efficiency for up to 10 years and shall not be affected by external conditions such as oxygen, moisture, etc. Possible solutions to this problem include more stable photoactive materials,[12] inverse architectures,[13] interfacial layers for improved charge extraction,[14] and device encapsulation.[15] In addition, these factors must be considered in the context of low-cost and high-throughput manufacturing. To identify and exploit the most effective architectures again requires a fundamental understanding of the loss mechanisms which have so far limited device lifetime and stability.

Several studies have examined the chemical and physical degradation of the photoactive layer as well as the interfacial contacts where charge is extracted in these devices.[8,16,17] The conjugated polymers that are used in the photoactive layer are susceptible to photochemical modification in the presence of water and can also undergo a reversible doping in the presence of oxygen while under illumination. These two atmospheric contaminants can also react with the interfacial layer(s) and charge extracting electrodes. All of these effects have been shown to reduce device efficiency as reflected by a reduction in the measured short-circuit current and fill factor. In addition, chemical and physical degradation of the photoactive layer can promote modification of the interface at the charge collecting electrodes, which can be further accelerated for photoactive layers prepared using low PCBM contents.[18]

Intensity modulated photocurrent spectroscopy (IMPS) is a powerful characterization technique that has recently been shown to be an effective method for the investigation of charge transport and carrier recombination in organic solar cells, particularly as related to device stability.[1] Using this technique, it is possible to separate the contributions of geminate and nongeminate recombination since they occur on a different time scale. This opens a way to better understand the effect of these processes on the device efficiency. Recently, we demonstrated using IMPS and its sister technique, intensity modulated photovoltage spectroscopy (IMVS), that interfacial nongeminate recombination plays an important role in low efficiency of bulk heterojunction organic solar cells.[1] Furthermore, it was found that the recombination rate actually increased with device aging and the illumination intensity,[1] which suggested that a large density of interfacial states able to trap photogenerated carriers was formed under illumination. Similar observations have been made recently by other authors using IMPS[19,20] and related techniques such as intensity-modulated scanning Kelvin probe microscopy[21] and IMVS[22] for organic bulk heterojunction solar cells as well as for other solar cell types like perovskites.[23] An increase in the recombination rate upon degradation and exposure to ambient air was also recently noted using IMPS.[24]

In this context it is important to better understand the nature of the states that are formed upon degradation and augment the recombination losses. In the case of nongeminate recombination in donor−acceptor materials, the recombining carriers are those that are formed upon dissociation of primary excitons, that is, holes in the P3HT phase and electrons captured by the PCBM acceptor phase. Using this argument, we suggested in our previous work that these sites could be located either at the P3HT:PCBM internal heterojunction interface or at the Al contact where both P3HT and PCBM domains come close to the contact.[1] Later, Luther and co-workers[24] attributed the occurrence of nongeminate recombination to formation of certain deep traps inside the photovoltaic layer. However, their treatment considered photogeneration, transport, and recombination inside the photovoltaic layer as a whole and so the exact location of those traps within the photovoltaic layer could not be clarified. For instance, their model could not distinguish between interfacial recombination at P3HT/PCBM bulk heterojunction and bulk recombination inside, for instance, phase-segregated P3HT or PCBM grains. Very recently, Grey and co-workers[25,26] reported their results of intensity modulated photocurrent imaging of P3HT/PCBM bulk heterojunction solar cells where they directly observed enhanced nongeminate recombination rates at the interfaces between P3HT and PCBM domains, which were presumably caused by formation of interfacial states that promoted recombination. However, the origin of such states still remains unexplored.

In this work, we further explore this research direction and confirm, using a detailed analysis of the IMPS data at various light intensities, that interfacial recombination indeed occurs at the interfacial states at the P3HT/PCBM interface. These states are not involved in carrier extraction and act as recombination centers only. Furthermore, the occurrence of these states is found to be directly related to exposure of cells to atmospheric contaminants. Exclusion of atmospheric exposure through encapsulation was effective in eliminating interfacial recombination, whereas devices that were not encapsulated demonstrated a significant amount of interfacial recombination that was dependent on the photoactive layer composition. Furthermore, it was found that even a brief exposure of nonencapsulated devices to atmospheric conditions was sufficient to form a significant number of interfacial states that continued to act as efficient recombination centers and contributed to continuing degradation of the cell performance even without any further atmospheric exposure. The devices with low PCBM loading ratio were shown to suffer most from this effect, thus suggesting the need of using higher PCBM loading ratios to ensure the long-term stability of bulk heterojunction solar cells.

2. EXPERIMENTAL SECTION

2.1. Materials. ITO-coated glass substrates (CEC20S, ≤20 Ω sq^{-1}) from Präzisions Glass & Optik GmbH were cleaned in an ultrasonic bath with sequentially, detergent deionized water (DI water), acetone, and isopropyl alcohol, followed by UV ozone cleaning for 10 min. PEDOT:PSS (Bayer Baytron Co.), P3HT (98.5% regioregular from Sigma-Aldrich Co.), and PCBM (Solenne BV Co.) were used as received without further purification.

2.2. Device Fabrication. Bulk heterojunction solar cells were fabricated using an ITO/PEDOT:PSS/P3HT:PCBM/Al architecture. A PEDOT:PSS hole transport layer was spin-coated onto ITO and annealed in an oven at 120 °C for 15 min prior to spin-coating the P3HT:PCBM photoactive layer. The ratio of the P3HT:PCBM photoactive layer was varied from 1:0.5 to 1:0.8 by varying the mass ratio of P3HT and PCBM dissolved in dichlorobenzene leading to films with a thickness of approximately 120 nm.[27] The total mass of the P3HT and PCBM was always 40 mg mL^{-1}. An aluminum cathode was evaporated on-top of the photoactive layer to complete the cell. The completed devices were annealed at 150 °C for 30 min in an inert atmosphere. They were not exposed to ambient conditions at any time during fabrication. For some of the cells, a UV-curable epoxy resin was used to encapsulate the devices. Devices were fabricated at the University of Strasbourg, France. Completed devices were placed in a vacuum sealed container and transported to the University of Western Ontario, Canada, for IMPS measurements. However, the container

DOI: 10.1021/acsami.6b12345
ACS Appl. Mater. Interfaces XXXX, XXX, XXX−XXX

Table 1. Device Parameters for Bulk Heterojunction Devices Measured Shortly after Fabrication at the University of Strasbourg (AM 1.5) and after the Transportation to the University of Western Ontario (Laser Diode)

	encapsulated				nonencapsulated			
P3HT:PCBM	1:0.5	1:0.6	1:0.7	1:0.8	1:0.5	1:0.6	1:0.7	1:0.8
AM 1.5								
j_{SC}/mA cm^{-2}	6.78	8.24	7.41	6.92	7.41	8.66	8.49	7.47
V_{OC}/V	0.54	0.53	0.56	0.53	0.49	0.53	0.51	0.56
efficiency/%	1.95	2.36	2.45	2.16	1.73	2.51	2.4	2.46
fill factor/%	53.2	53.8	59.6	59.8	47.5	55.2	55.8	59.2
laser diode								
j_{SC}/mA cm^{-2}	4.21	6.52	5.58	6.69	0.532	0.407	1.41	4.17
V_{OC}/V	0.52	0.50	0.54	0.56	0.42	0.38	0.43	0.46
efficiency/%	0.99	1.60	1.59	1.86	0.04	0.05	0.15	0.67
fill factor/%	51.9	55.8	60.4	57.1	18.8	33.3	27.8	39.4

used could not support high vacuum, and therefore the cells were necessarily exposed to some atmospheric contamination during transportation. Upon arrival to the University of Western Ontario, all cells were immediately placed in a nitrogen-purged glovebox or an Ar-purged environmental chamber and were not exposed to atmospheric conditions again.

2.3. Steady-State *J*−*V* Measurements. A solar simulator was used for AM 1.5 (100 mW cm^{-2}) photocurrent measurements at the University of Strasbourg, France. Photocurrent measurements at the University of Western Ontario were performed using a 20 mW monochromatic 405 nm laser diode (LD1510, Power technology). This light source was used to ensure consistency with IMPS measurements, which were performed using the laser diode light source. The range of light intensities used was 3.07×10^{16}−2.95×10^{17} photons cm^{-2} s^{-1}, which corresponds to an incident power of 15−145 mW cm^{-2}. Steady-state *J*−*V* measurements were collected using a PAR 263A potentiostat−galvanostat (Princeton Applied Research) that was controlled using version 3.1 CorrWare software (Scribner Associates Inc.). Aging of the photovoltaic devices was done at room temperature in a nitrogen-purged glovebox for 30 days.

2.4. Intensity Modulated Photocurrent Measurements. Intensity modulated photocurrent/photovoltage measurements were made using either a PAR 263A potentiostat−galvanostat (Princeton Applied Research) coupled with a Solartron 1250 frequency response analyzer or a stand-alone Solartron 1260 frequency response analyzer. The dc light intensity was varied from 3.07×10^{16} to 2.95×10^{17} photons s^{-1} cm^{-2}, while the ac one was kept constant at 3.07×10^{16} s^{-1} cm^{-2}, which was determined to be small enough to ensure a linear cell response. All measurements were performed in an Ar purged environmental chamber equipped with an optical window.

3. RESULTS AND DISCUSSION

3.1. Steady-State Measurements of Bulk Heterojunction Solar Cells. A series of bulk heterojunction devices containing varying amounts of PCBM were fabricated and investigated using steady state current−voltage measurements as well as the nonsteady state technique intensity modulated photocurrent spectroscopy. Mass ratios of P3HT to PCBM of 1:0.5, 1:0.6, 1:0.7, and 1:0.8 were used. It has been shown that low PCBM contents give rise to lower efficiencies than higher PCBM contents, with the optimal mass ratio being in the range of 1:0.8 to 1:1.[28] While efficiencies as high as 5% can be obtained for the P3HT:PCBM system through judicious modification of the processing parameters, the majority of reports using P3HT with PCBM typically exhibit device efficiencies in the range of 2−3.5%. For the photoactive layer compositions used in this work, device efficiencies in the range of 1.7−2.5% were obtained under AM 1.5 solar simulator conditions immediately following device fabrication (see Table 1). The efficiencies were similar for both encapsulated and nonencapsulated devices. The lowest PCBM content films (1:0.5) exhibited the lowest efficiencies of 1.7%, while all other compositions exhibited efficiencies of approximately 2.5%. The lower efficiency observed for the 1:0.5 P3HT:PCBM mass ratio is attributed to the inefficient formation of a percolation network throughout the film.

Shortly following the solar simulator measurements, but at a different location at the University of Western Ontario, London, Canada (which therefore required the cells to be packed into a transfer vessel and transported to this location; see Experimental Section for further details), the devices were again measured using a monochromatic laser diode (λ = 405 nm), and their efficiencies were determined from the corresponding *J*−*V* plots. Measurements were made using this light source because it was also used for the IMPS measurements that are discussed further below. The results are also presented in Table 1.

One can see from the table that encapsulated devices showed similar efficiencies when measured shortly following fabrication and after the transportation. A certain decrease in the efficiency when using the monochromatic laser diode was most likely due to a shorter wavelength of the laser diode light. However, nonencapsulated devices showed a substantial reduction in efficiency that was dependent on PCBM content in the films. The cell efficiency was also found to decrease after further aging for 30 days in the dark (Table 2) despite the fact that the cells were stored in inert atmosphere in a nitrogen-filled glovebox during all this time.

This trend is also illustrated in Figure 1 that shows *J*−*V* plots of bulk heterojunction devices for two P3HT:PCBM mass ratios measured after transportation to the University of Western Ontario. The cells with other P3HT:PCBM mass ratios showed similar behavior (see Supporting Information). Curves 1 and 2 were measured right upon receiving the devices

Table 2. Device Parameters for Bulk Heterojunction Devices Measured after Aging in Inert Atmosphere at the University of Western Ontario

	nonencapsulated (aged)			
P3HT:PCBM	1:0.5	1:0.6	1:0.7	1:0.8
laser diode				
j_{SC}/mA cm^{-2}	0.202	0.454	0.897	2.27
V_{OC}/V	0.48	0.42	0.44	0.54
efficiency/%	0.01	0.03	0.06	0.21
fill factor/%	10.4	20.6	18.9	19.8

DOI: 10.1021/acsami.6b12345
ACS Appl. Mater. Interfaces XXXX, XXX, XXX−XXX

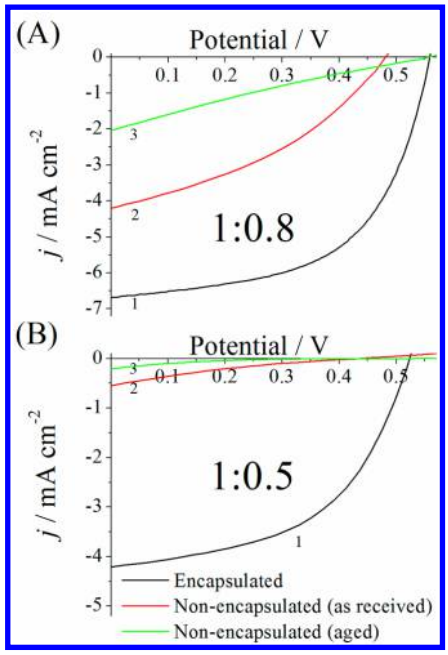

Figure 1. *J*–*V* plots of bulk heterojunction devices containing a P3HT:PCBM mass ratio of (A) 1:0.8 and (B) 1:0.5 measured using a 405 nm laser diode at the University of Western Ontario. The dc light intensity was 1.62×10^{17} s^{-1} cm^{-2}. Curves 1 and 2 correspond to encapsulated and nonencapsulated as-received devices, whereas curve 3 corresponds to nonencapsulated device that was aged for 30 days but without further exposure to atmospheric conditions.

and correspond to encapsulated and nonencapsulated cells, respectively, whereas curve 3 corresponds to a nonencapsulated device that was aged for 30 days but without further exposure to atmospheric conditions.

Therefore, the data show that encapsulation plays a very significant role in the device efficiency. Whereas all devices showed comparable efficiencies right after fabrication, devices that were not encapsulated exhibited a substantial decrease in efficiency upon transportation compared to devices that were encapsulated. The effects were especially severe for such parameters as the short-circuit current density j_{SC} and fill factor. Therefore, the reduction in the cell efficiency observed upon transportation for nonencapsulated cells should be related to the exposure to atmospheric contaminants such as oxygen and moisture that could not be completely eliminated during transportation. Furthermore, even though all devices received at the University of Western Ontario were continuously stored in a glovebox under nitrogen upon their delivery without further exposure to atmospheric contaminants, nonencapsulated cells continued to undergo further deterioration of their performance, as opposed to encapsulated cells.

It has been shown that atmospheric oxygen or moisture, if present, are able to penetrate into the photoactive layer through grain boundaries and pinholes present in the aluminum cathode layer.[8] Our data suggest that even short exposure to these contaminants is sufficient to modify the photovoltaic layer in such a way as to cause continuous and irreversible degradation. One possible mechanism of such effect may be formation of a large number of interfacial states inside the photovoltaic layer due to reactions with oxygen and moisture, especially at the grain boundaries. Such interfacial states, if present, would strongly enhance the rate of the interfacial recombination and thus decrease the cell efficiency. In order to investigate this hypothesis, we performed non-steady-state intensity modulated photocurrent (IMPS) measurements since IMPS is one of the most powerful techniques for studies of the interfacial recombination in various photovoltaic materials.

3.2. Intensity Modulated Photocurrent Spectroscopy (IMPS) of Encapsulated and Nonencapsulated Devices.

Figure 2 presents typical IMPS plots obtained in short-circuit

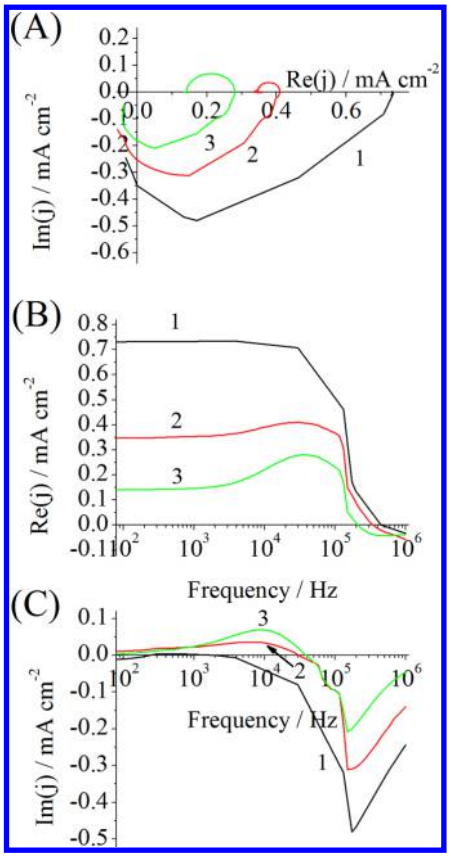

Figure 2. Typical IMPS spectra in (A) Nyquist and (B, C) Bode plot representation obtained in short-circuit conditions for (1) as-received encapsulated cell and nonencapsulated cell both (2) as-received and (3) upon aging in nitrogen atmosphere for 30 days. The P3HT:PCMB ratio was 1:0.8, and the dc light intensity was 1.62×10^{17} s^{-1} cm^{-2}.

conditions at the same light intensity for as-received encapsulated cell and nonencapsulated cells as well as nonencapsulated cell upon aging in nitrogen atmosphere for 30 days. Similar data were obtained for other cells and light intensities (see the complete set of data in the Supporting Information). The IMPS spectra are given both in Nyquist and Bode plot representation, that is, on the complex plane and as separated dependencies of the real and imaginary components of the photocurrent on the light modulation frequency. An important difference is immediately seen between encapsulated and nonencapsulated cells: the spectra for nonencapsulated cell show characteristic arcs in quadrant I of the complex plane (Nyquist representation) that become more pronounced upon aging, whereas the spectrum for encapsulated cell does not show this feature. In the Bode representation, the imaginary component of the ac photocurrent for the encapsulated cell (curve 1) remains negative at all modulation frequencies, whereas the imaginary components for nonencapsulated cells (curves 2 and 3) change the sign and become positive at lower frequencies (photocurrent leads the light intensity). Such arcs

DOI: 10.1021/acsami.6b12345
ACS Appl. Mater. Interfaces XXXX, XXX, XXX–XXX

as well as corresponding positive phase shifts are typical manifestations of the occurrence of interfacial recombination.[1,29−34] All nonencapsulated cells demonstrated such arcs in our measurements, whereas all encapsulated cells lacked this feature. Therefore, we must draw a very important conclusion that encapsulation appeared to be a very effective measure to prevent the occurrence of interfacial recombination in bulk heterojunction devices. On the other hand, even brief exposure to atmospheric contaminants during device transportation was sufficient to cause the occurrence of pronounced interfacial recombination in our devices, as evidenced by IMPS data.

The occurrence of interfacial recombination in nonencapsulated devices upon exposure to atmospheric contaminants can explain a pronounced reduction in the short-circuit current density as revealed by the data of Tables 1 and 2. In IMPS measurements, the short-circuit current density measured under continuous illumination is represented by the low-frequency limit of the ac photocurrent ReJ_0. It can be evaluated, for example, from the low-frequency plateaus in Figure 2B. One can see that the occurrence of interfacial recombination in nonencapsulated devices decreases this parameter significantly, thus indicating additional losses that occur in the device due to interfacial recombination.

Figure 2, curve 3, shows the IMPS data for the same cell as in curve 2 but measured following aging in a controlled glovebox environment that limited further atmospheric exposure. One can see that the aged cells show a reduction in both their high-frequency and low-frequency values for the real component of the photocurrent, indicating both a reduction in the number of generated charge carriers and their poorer extraction with aging (see below for more discussion). This is consistent with the results of the steady-state measurements. Also, the frequency at the maximum for the imaginary photocurrent has shifted to a higher frequency for the aged cell in comparison to the as-received cell. This indicates that the reason for the decrease in performance upon cell aging is an increase in the rate of interfacial recombination. The same fact was observed in our previous work.[1] The size of the characteristic arc for the aged cell is much larger and the ReJ_0 value is much lower, indicating a further increase in the fraction of charge carriers that are lost to interfacial recombination.

Importantly, this increase in the recombination losses in aged cells occurred even without further exposure to atmospheric contaminants. This fact highlights the importance of encapsulation to prevent the recombination losses in bulk heterojunction devices. Furthermore, since IMPS spectra are sensitive to the presence of interfacial states and can detect interfacial recombination, IMPS can be used as a powerful diagnostic tool to predict the performance of organic solar cells. All devices in this study that initially showed the presence of interfacial states as indicated by characteristic semicircle arcs in the I quadrant of the IMPS spectra demonstrated deterioration of their performance due to enhanced interfacial recombination, even without further exposure to atmospheric contaminations.

3.3. Effect of the Light Intensity. Figure 3 presents typical IMPS spectra in the Nyquist and Bode plot representations obtained for a nonencapsulated device at different dc light intensities for a 1:0.7 P3HT:PCBM mass ratio. The cells with other P3HT:PCBM mass ratios showed similar results (see Table 3). The IMPS plots follow similar trends to those observed with increasing dc light intensity in our previous study.[1] Specifically, the maximum of the imaginary

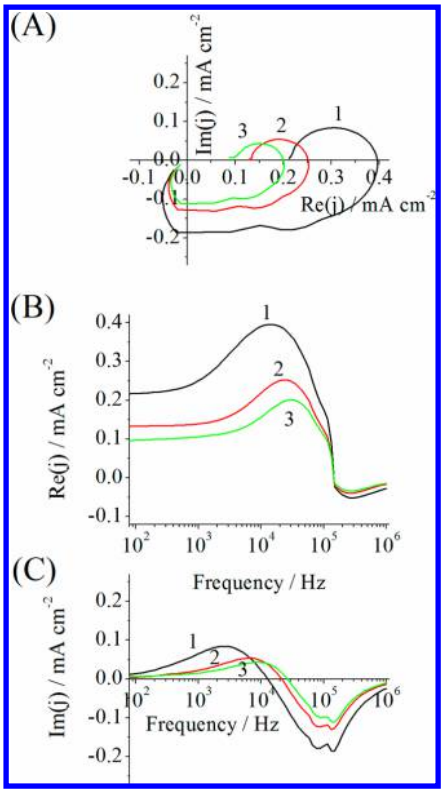

Figure 3. Typical IMPS spectra obtained in short-circuit conditions for a P3HT:PCBM ratio of 1:0.7 in (A) Nyquist and (B, C) Bode plot representation. The dc light intensity used was (1) 3.07×10^{16}, (2) 1.62×10^{17}, and (3) 2.95×10^{17} s^{-1} cm^{-2}.

photocurrent in quadrant 1 shifts to higher frequencies with increasing dc light intensity as shown in Figure 3C. The frequency at the maximum of the imaginary photocurrent is represented by ω^* and corresponds to the pseudo-first-order rate constant for interfacial recombination.

Figure 4 shows the frequency corresponding to the maximum of the imaginary photocurrent in quadrant I for all cells as a function of dc light intensity. It can be seen that the recombination rate increases with increasing dc light intensity for all cells, but it does not appear to show a significant variation or dependence on the PCBM content. It is important to point out that the pseudo-first-order rate constant ω^* implicitly includes the majority carrier concentration. Therefore, these data suggest that recombination involves not only photogenerated minority carriers but photogenerated majority carriers (holes) as well. These carriers should be located in the p-type P3HT phase. Normally, photogenerated majority carriers are rapidly swept away by the electric field; however, the carrier mobilities in conjugated organic semiconductors such as P3HT could be lower and thus some photogenerated majority carriers may be trapped near the interface and contribute to the recombination with photogenerated electrons. Our data suggest that this is a predominant recombination mechanism since the values of the recombination rate constant under illumination are significantly higher than those in the dark (found as the extrapolation of the recombination rate to zero light intensity, Figure 4).

The values of the ac photocurrent also follow the trend (Figure 3). An increase in the dc light intensity results in a reduction in both the real and imaginary components of the photocurrent over a wide frequency range. This means that

DOI: 10.1021/acsami.6b12345
ACS Appl. Mater. Interfaces XXXX, XXX, XXX−XXX

Table 3. Values for the Low-Frequency Limit ReJ_0, the High-Frequency Limit g_{ac}, the Frequency at the Maximum of the Imaginary Photocurrent in the First Quadrant ω^*, and the Fraction of the Carriers Captured at the Interfacial States γ Determined from the IMPS Plots

	as-received				aged			
P3HT:PCBM	1:0.5	1:0.6	1:0.7	1:0.8	1:0.5	1:0.6	1:0.7	1:0.8
g_{ac}/mA cm^{-2}	0.186	0.342	0.250	0.408	0.202	0.238	0.262	0.280
ReJ_0/mA cm^{-2}	0.082	0.218	0.133	0.348	0.0110	0.0780	0.090	0.141
ω^*/s^{-1}	6660	6660	5800	5800	8730	8730	8730	8730
γ	0.56	0.37	0.48	0.17	0.94	0.68	0.65	0.50

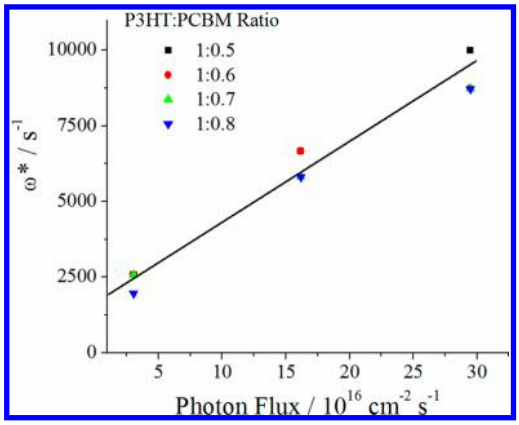

Figure 4. Value of the rate constant for recombination ω^* for all the P3HT:PCBM mass ratios for as received devices as a function of the dc light intensity. The line is not a fit and is a guide for the eyes.

more carriers are lost to recombination at higher light intensities, again suggesting the involvement of photogenerated majority carriers trapped in P3HT phase. Importantly, the photocurrent decreases over a wider frequency range than those attributed to interfacial recombination. This fact suggests that trapping of photogenerated majority carriers occurs not only near the interface but also in the bulk of P3HT phase and contribute to both interfacial and bulk recombination losses.

The independence of ω^* of the PCBM content for a given dc light intensity suggests that the rate constant for the interfacial recombination does not depend on the PCBM or P3HT concentrations. However, the short-circuit current densities for nonencapsulated devices do exhibit a dependence on the PCBM content as observed in their steady-state $J-V$ plots (Table 1 and Supporting Information), with films containing a greater fraction of PCBM showing higher efficiencies. It could be expected that the recombination rate constant would increase for decreasing PCBM contents if interfacial recombination were occurring at the PCBM/Al interface, which would lead to a dependence of the recombination rate constant on the PCBM content in the active layer and at the interface. This is discussed in the next section.

3.4. Effect of the PCBM Content. Figure 5 shows the IMPS spectra for P3HT:PCBM films with increasing ratios of PCBM content in the photoactive layer. Several trends can be observed in these figures. The Bode plot in Figure 5B shows that for increasing PCBM content the low-frequency portion of the real photocurrent is greater in magnitude, which is similar to the trend observed in the steady state $J-V$ plots (Figure 1) above. As well, Figure 5C shows that ω^* does not vary significantly with the P3HT:PCBM ratio, which would suggest that an increase in the rate constant for recombination with

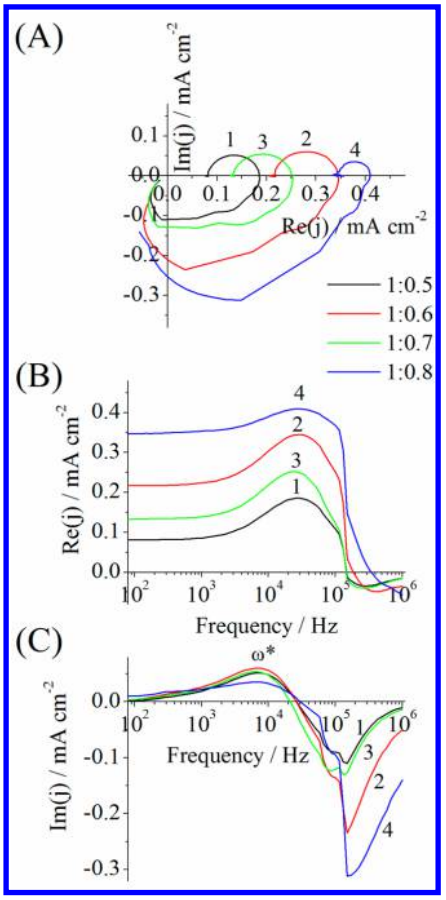

Figure 5. Experimental IMPS spectra for as-received devices obtained in short-circuit conditions for P3HT:PCBM ratios of (1) 1:0.5, (2) 1:0.6, (3) 1:0.7, and (4) 1:0.8 in (A) Nyquist and (B, C) Bode plot representation. The dc light intensity for all spectra was 1.62×10^{17} s^{-1} cm^{-2}.

decreasing PCBM content cannot explain the decrease in device efficiency. The shape of the IMPS spectra (Figure 5A) in the first quadrant shows that cells with higher PCBM content exhibit a smaller semicircle than those with lower PCBM content. This is indicative of reduced recombination in the devices, but this is not accompanied by a change in the value of ω^* as observed in Figure 5C.

Figure 6 shows the normalized low frequency portions of the IMPS spectra for a series of P3HT:PCBM cells at a light intensity of 1.62×10^{17} s^{-1} cm^{-2}. Normalizing the data allows a comparison between the size and shape of the spectra, which are due to differences in interfacial recombination. One can see that the semicircles in the first quadrant increase in size with decreasing PCBM content, which indicates that an increasing number of charge carriers are lost to interfacial recombination

DOI: 10.1021/acsami.6b12345
ACS Appl. Mater. Interfaces XXXX, XXX, XXX−XXX

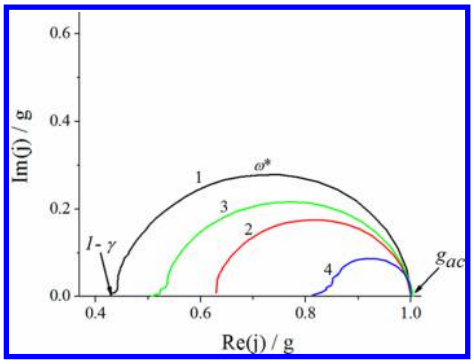

Figure 6. Normalized IMPS spectra for as received devices obtained at short-circuit conditions for P3HT:PCBM ratios of (1) 1:0.5, (2) 1:0.6, (3) 1:0.7, and (4) 1:0.8. The dc light intensity for all spectra was 1.62 × 10^{-17} s^{-1} cm^{-2}. The high-frequency intercept g_{ac}, low-frequency intercept $1 - \gamma$, and the maximum of the imaginary photocurrent ω^* are indicated.

for lower PCBM containing films. To further understand the role of interfacial recombination, it is useful to define three parameters as indicated in Figure 6. The three parameters are the (1) high frequency intercept g_{ac}, (2) the low frequency intercept ReJ_0, and (3) the frequency corresponding to the maximum of the imaginary photocurrent in the first quadrant ω^*.

The high-frequency intercept is determined by the point in the complex plane plots of Figure 5A at which the imaginary photocurrent crosses over from quadrant IV to quadrant I. It can also be determined as the maximum value of the real photocurrent, e.g., as in Figure 5B. This parameter is indicated in Figure 6 as g_{ac}, which is unity in the normalized plots, and represents the maximum attainable photocurrent if no interfacial recombination were occurring. The next parameter is the frequency that corresponds to the maximum for the imaginary photocurrent in quadrant I, indicated by ω^* in Figure 6. The final parameter is the real photocurrent ReJ_0 measured at low frequency, which represents the situation where the steady-state photocurrent would be measured. As has been already discussed, it can be also determined from the low-frequency plateau on the frequency dependence of the real component of the photocurrent (e.g., Figure 5B). In the normalized plots, this is the fraction of charge carriers that are not lost to interfacial recombination and are extracted at the electrode. This parameter can be represented by the product $g_{ac}(1 - \gamma)$, where γ denotes the fraction of charge carriers that recombine. A smaller value of $g_{ac}(1 - \gamma)$ indicates a greater number of charge carriers that are lost to interfacial recombination. The parameters ReJ_0, g_{ac}, and $g_{ac}(1 - \gamma)$ are related through the following expression:

$$ReJ_0 = g_{ac}(1 - \gamma) \quad (1)$$

which can be arranged in the following form:

$$1 - \gamma = ReJ_0/g_{ac} \quad (2)$$

The values of this parameter are given in Table 3 along with the experimental values for the low-frequency limit of the photocurrent ReJ_0, high-frequency limit of the photocurrent g_{ac}, and the frequency corresponding to the maximum of the imaginary photocurrent in the first quadrant ω^* determined from the IMPS plots.

It is clear from Figure 6 and Table 3 that the value $ReJ_0 = g_{ac}(1 - \gamma)$ increases with the amount of PCBM in the film indicating that the contribution of the interfacial recombination increases at low PCBM contents, which is reflected in a lower device efficiency. Therefore, we conclude that while the rate of interfacial recombination per se does not depend significantly on the PCBM content, as suggested by the independence of the parameter ω^*, an increase in the PCBM content reduces the recombination losses by decreasing the fraction γ of photogenerated carriers trapped at the interfacial states. An obvious explanation for this effect is that an increase in the PCBM content enhances the charge separation and extraction, which is a competing process to the interfacial recombination. Incidentally, this is an indication of the localization of interfacial recombination at the P3HT/PCBM interface. This is explored in detail in the next section. Furthermore, an increase in the PCBM content increases the generation current g_{ac}, thus again suggesting an increase in the efficiency of exciton dissociation with the PCBM content or improved bulk transport.

These conclusions are also supported by the observations of the changes in the steady-state $J-V$ curves with PCBM content (Tables 1 and 2). One can see that despite an overall decrease in the efficiency, the short-circuit current density and the fill factor were still increasing with the PCBM content for both as-received and aged cells. However, aged cells show a significantly decreased value of the short-circuit current density compared to the as-received cells, with the differences becoming more pronounced at higher PCBM contents. This correlates well with the behavior of parameters $g_{ac}(1 - \gamma)$ and ReJ_0 derived from IMPS spectra (Table 3) and can be also explained by enhanced charge separation and extraction in the photovoltaic layer. Importantly, encapsulated devices as well as as-prepared nonencapsulated devices before transportation (Table 1) did not exhibit such dependence on the PCBM content, suggesting that differences in phase segregation, morphology, or interfacial mixing between the two materials are not the origin of the observed dependence of the device efficiency on the PCBM content. Rather, the latter should be attributed to the formation of the interfacial states upon exposure to the atmospheric contaminants and competition between carrier separation/extraction and their capture at the interfacial states. The same mechanism should be responsible for the observed changes in the fill factor.

The open circuit voltage (Tables 1 and 2) does not vary significantly with PCBM content and even increases slightly for aged cells. The relative independence of the open circuit voltage with the PCBM content can be expected as its value is a function of the difference between the LUMO level of the PCBM and HOMO level of P3HT, which does not change with variations of the PCBM content. A slight increase in V_{OC} with aging can be attributed to an increased shunt resistance of the film that occurs due to film degradation.[10]

3.5. Analysis of the Recombination Mechanism from Parameters Derived from IMPS Measurements. To better understand which interface is primarily responsible for the occurrence of the interfacial recombination, PCBM/Al or P3HT/PCBM, two separate models are used to interpret the IMPS spectra that correspond to different interfaces where recombination could occur. In both models it is important to state that we are discussing the trapping of an electron at an interfacial state. In this case, recombination of photoexcited electrons cannot occur at the interfacial states formed between P3HT and the aluminum cathode, as P3HT is a hole majority

DOI: 10.1021/acsami.6b12345
ACS Appl. Mater. Interfaces XXXX, XXX, XXX−XXX

carrier with low exciton dissociation efficiency on its own and will have no or very few free photogenerated electrons. Therefore, electron recombination from P3HT at the aluminum cathode cannot explain the significant amount of charge that is being generated and collected in our measurements. The two remaining interfaces where interfacial recombination can occur are the P3HT/PCBM interface or the PCBM/Al interface. These two separate cases are illustrated below in Figure 7.

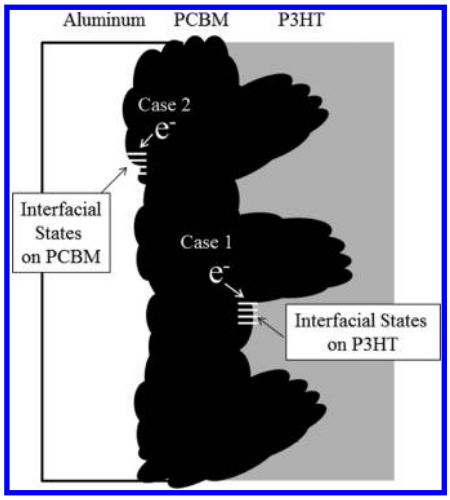

Figure 7. Schematic showing the possible interfaces where interfacial recombination may occur in a bulk heterojunction P3HT:PCBM device.

Case 1: No Extraction from Interfacial States. In case 1, the interfacial states responsible for the recombination are assumed to be located at the P3HT/PCBM interface. Therefore, all carriers trapped at the interfacial states recombine and cannot be extracted. In this case, the low-frequency intercept of the real component of the photocurrent $ReJ_0 = g_{ac}(1 - \gamma)$ will correspond to carriers that escape trapping at the interfacial states and are extracted directly at the PCBM/Al interface. The corresponding fraction of carriers that escape trapping and recombination will be equal to $1 - \gamma$ as described above. Figure 8A plots the experimental values for the low- and high-frequency intercepts in quadrant I as a function of the PCBM content for aged cells (data for as-received cells demonstrated similar behavior and are not shown), while Figure 8B plots the corresponding values of $1 - \gamma$ for as-received and aged cells.

From Figure 8A one can see that g_{ac} decreases with decreasing PCBM content, indicating that carriers are not being generated as efficiently and/or being lost to bulk recombination as the PCBM content in the film is decreased. However, examination of the value of ReJ_0 in Figure 8A shows that its value decreases much more rapidly compared to g_{ac} with decreasing PCBM content. The difference in the slope for the values of ReJ_0 compared to g_{ac} demonstrates that losses due to interfacial recombination are dramatically enhanced for devices with low PCBM content.

Figure 8B plots the value of $1 - \gamma$, which represents the fraction of photogenerated charges that are extracted at the electrode. One can see that this value increases significantly with an increase in the PCBM content. This indicates enhanced carrier extraction in the device. At the same time, as was shown above, the pseudo-first-order rate constant for interfacial recombination did not depend or showed only a slight

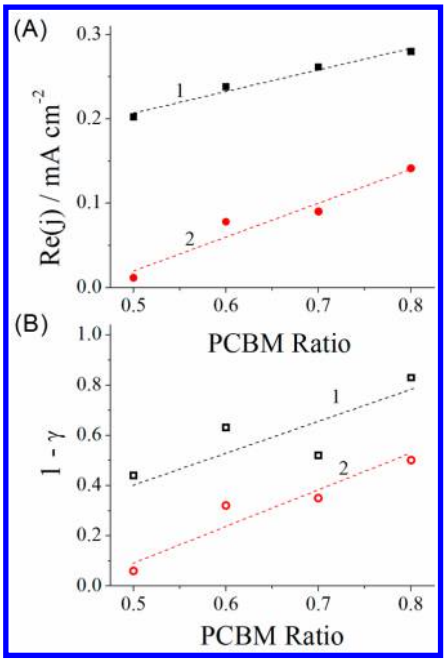

Figure 8. (A) Values for the (1) high-frequency intercept g_{ac} and the (2) low-frequency intercept ReJ_0 for aged cells as a function of PCBM content in the film. (B) Fraction of charge carriers collected at the contacts $1 - \gamma$ as a function of PCBM content for (1) as-received cells and (2) aged cells. A light intensity of 1.62×10^{17} s^{-1} cm^{-2} was used.

dependence on the PCBM content in the film. Taken together, these two facts indicate that an increase in the cell efficiency at elevated PCBM contents is not due to suppression of interfacial recombination but rather originates from enhanced carrier extraction at the PCBM/Al interface.

This mechanism is further corroborated by the light intensity dependencies of parameters $1 - \gamma$ and ω^*. As has been discussed above (see Figure 4), the parameter ω^* that represents in this model the pseudo-first-order recombination rate constant increases significantly with the light intensity, whereas the parameter $1 - \gamma$ was found to be virtually independent of the light intensity. The light intensity dependence of ω^* was attributed to the majority carriers (holes) trapped in the P3HT phase. Therefore, these facts suggest that carrier extraction indeed should occur at the PCBM/Al interface where no contribution from carriers trapped in P3HT could be expected, whereas the recombination should occur at the internal PCBM/P3HT interface between phase segregated P3HT and PCBM domains.

The rate of interfacial recombination increases with aging, which suggests either further chemical modification of the active layer or morphological changes in the film/at the interfaces. While oxygen can modify the conjugated polymer under illumination, this process does not occur in the dark.[16] These devices were stored in a glovebox in the dark during aging and photochemical modification is not likely in this case. At the same time, our results do show that exposure to oxygen and moisture triggers certain processes at the interfaces/grain boundaries between the P3HT and PCBM phases that promote continuing formation of interfacial states even without further atmospheric exposure. The interfacial states then start to trap more photoexcited carriers, thus increasing the recombination losses. The specific mechanisms may involve chemical modification of P3HT and/or PCBM at the grain boundaries

DOI: 10.1021/acsami.6b12345
ACS Appl. Mater. Interfaces XXXX, XXX, XXX−XXX

Table 4. Values for the Rate Constant for Charge Transfer k_{tr} from the Interfacial States to the Al Electrode along with a Rate Constant for Interfacial Recombination k_{rec}

	nonencapsulated (as-received)							
	k_{tr}				k_{rec}			
P3HT:PCBM	1:0.5	1:0.6	1:0.7	1:0.8	1:0.5	1:0.6	1:0.7	1:0.8
photon flux/cm^2 s^{-1}								
3.07×10^{16}	1073	1521	1382	1923	1508	1060	1199	331
1.62×10^{17}	3267	4058	3450	6339	4360	2602	3211	1288
2.95×10^{17}	2298	5752	3683	7505	7702	2981	5051	2495
	nonencapsulated (aged)							
	k_{tr}				k_{rec}			
P3HT:PCBM	1:0.5	1:0.6	1:0.7	1:0.8	1:0.5	1:0.6	1:0.7	1:0.8
photon flux/cm^2 s^{-1}								
3.07×10^{16}	418	1290	1150	1415	2537	2094	1805	1166
1.62×10^{17}	491	2846	2943	4228	8243	5887	5790	4505
2.95×10^{17}	400	3452	2812	5835	11050	9659	8638	7276

between the P3HT and PCBM rich domains; however, their clarification requires further studies.

It has been shown that the addition of a fullerene (C_{60}) layer between the photoactive layer and cathode led to more reproducible bulk heterojunction organic photovoltaic devices.[35] This increase in reproducibility was attributed to the formation of a more stable interface between the photoactive layer and cathode material. It has also been shown that a C_{60} layer is able to prevent the diffusion of oxygen into the active layer, which would help to reduce degradation and interfacial recombination.[8] Taken into consideration our results presented here, it is possible that such an interfacial C_{60} layer can also modify the PCBM/Al interface and improve carrier extraction at it. It could be expected that stable bulk heterojunction films with lower PCBM contents could be prepared if an interfacial layer between the photoactive layer and cathode was incorporated and the morphology did not change significantly. This may be a useful consideration when evaluating alternative acceptor materials to exclude interfacial effects. In addition, this may provide new opportunities to engineer the morphology and composition of the photoactive layer using new materials, if high loading ratios are not required.

Case 2: All Carriers Are Extracted through Interfacial States Only. In the previous case it was assumed that carriers cannot be extracted once they become trapped at an interfacial site and the charge transfer occurs directly from PCBM to Al without involvement of interfacial states. Case 2 considers the opposite situation where photogenerated charge carriers are extracted through interfacial states only.[36] In this case there is a competition between charge carrier recombination and charge carrier transfer from the interfacial state, and the interfacial recombination would occur at the PCBM/Al interface where there is the possibility that there would be a competition between charge carrier recombination in PCBM or extraction at the aluminum electrode. Therefore, the parameter ω^* will no longer be simply a pseudo-first-order recombination rate constant and should incorporate two separate components that include a rate constant for charge transfer k_{tr} from the interfacial states to the Al electrode along with a rate constant for interfacial recombination k_{rec}. The values of these two rate constants can be determined from the experimental IMPS plots by taking the sum of the charge transfer rate constant and the interfacial recombination rate constant and equating them to ω^* as shown in eq 3:

$$\omega^* = k_{tr} + k_{rec} \tag{3}$$

where k_{tr} is the rate constant for charge transfer and k_{rec} is the rate constant for interfacial recombination. Separation of these two components requires knowledge of the low-frequency intercept of the real photocurrent, which represents the fraction of electrons that are collected at the electrode and do not recombine. Since case 2 assumes that all carriers are extracted through interfacial states, this fraction for this model is expressed as

$$ReJ_0 = g_{ac}k_{tr}/(k_{tr} + k_{rec}) \tag{4}$$

Using eqs 3 and 4, it is possible to determine k_{tr} from k_{rec} from the high and low frequency intercepts along with the frequency at the maximum of the imaginary component of the photocurrent for quadrant I. The corresponding values of k_{tr} from k_{rec} are shown in Table 4.

However, the analysis of the results for case 2 shows a light intensity dependence not only for the recombination rate constant k_{rec} but also for the rate constant of the charge extraction k_{tr}, which does not have a clear physical meaning. The recombination rate constant could depend on the light intensity through the contribution of the majority carriers trapped in the P3HT phase, as discussed above; however, this should not affect the values of the charge transfer rate constant since majority carriers are not involved in charge extraction that occurs at the PCBM/Al interface. This model also cannot explain the variations of the parameters of IMPS plots on the PCBM content. Therefore, we must conclude that case 2 is not corroborated by the experimental data and therefore the photoprocess in our devices should be described by the mechanism outlined in case 1. Namely, the interfacial states where the charge recombination occurs are located at the P3HT/PCBM and not the PCBM/Al interface; there is no charge extraction through these interfacial states; all charge is extracted directly from PCBM at the PCBM/Al interface. These conclusions have been recently corroborated by direct spatially resolved IMPS imaging of P3HT/PCBM solar cells[25,26] that showed high rates of recombination localized at the phase boundaries between P3HT aggregates and PCBM crystallites. This also suggests that the origin of the deep traps discussed in ref 24 is in fact related to interfacial states formed at the P3HT/PCBM internal bulk heterojunction interface.

DOI: 10.1021/acsami.6b12345
ACS Appl. Mater. Interfaces XXXX, XXX, XXX−XXX

4. CONCLUSIONS

Bulk heterojunction organic solar cells containing varying amounts of PCBM were investigated using steady-state $J-V$ measurements in combination with the non-steady-state technique, intensity modulated photocurrent spectroscopy (IMPS). It was found that effective encapsulation of the devices could prevent interfacial recombination from occurring. However, for devices that were not encapsulated it was shown that interfacial recombination represents a significant loss pathway for all PCBM contents. The enhanced recombination rate was attributed to interfacial state formation due to reactions with atmospheric oxygen and moisture.

Two possible mechanisms were considered to identify the sites where interfacial recombination was occurring. Detailed analysis of the IMPS data allowed us to determine that interfacial recombination occurs at the internal P3HT/PCBM interface and that this process is accelerated for lower PCBM contents because of less efficient extraction of photoexcited carriers. Photoactive layers with the highest PCBM content showed the greatest stability with time and exhibited reduced interfacial recombination. This fact highlights the stabilizing effect of PCBM in organic solar cells that is sometimes overlooked when considering alternative acceptor materials. At the same time, it also represents a possible limitation in the use of PCBM for further improvements in device efficiency due to its high loading ratio, while contributing a negligible amount toward light absorption and carrier generation. We also conclude that while the interfacial states are responsible for interfacial recombination and the associated losses, charge separation at the P3HT/PCBM bulk heterojunction does not involve those interfacial states. This fact is also important because it shows that the best way to improve the device efficiency is to suppress the formation of such interfacial states.

Our results highlight the utility in the use of IMPS for the characterization of various bulk heterojunction systems. In particular, since IMPS spectra are sensitive to the presence of interfacial states and can detect interfacial recombination, IMPS can be used as a powerful diagnostic tool to predict the performance of organic solar cells. All devices in this study that initially showed the presence of interfacial states as indicated by characteristic semicircle arcs in the I quadrant of the IMPS spectra demonstrated deterioration of their performance due to enhanced interfacial recombination, even without further exposure to atmospheric contaminations. At the same time, none of the encapsulated devices showed any such arcs in the IMPS spectra and their performance was stable with aging.

■ ASSOCIATED CONTENT

Supporting Information

The Supporting Information is available free of charge on the ACS Publications website at DOI: 10.1021/acsami.6b12345.

$J-V$ plots and IMPS spectra of encapsulated, non-encapsulated, and aged cells with varying P3HT:PCBM mass ratios (PDF)

■ AUTHOR INFORMATION

Corresponding Author

*E-mail osemenik@uwo.ca; Ph +1 519 661 2111, ext 82858; Fax +1 519 661 3022 (O.A.S.).

Present Address

J.C.B.: Département de Chimie, Université du Québec à Montréal, Succ. Centre-Ville, CP8888, Montréal, QC H3C3P8, Canada.

Notes

The authors declare no competing financial interest.

■ ACKNOWLEDGMENTS

O.A.S., J.C.B., and M.S. gratefully acknowledge the support by the Natural Sciences and Engineering Research Council of Canada (NSERC), Strategic Partnership Program, project STPGP 447326-13. O.A.S. and J.C.B. also acknowledge the support from NSERC Engage Program, project EGP 396334-10. O.A.S. also acknowledges his NSERC Discovery Individual grant. T.H. gratefully acknowledges the funding from CNRS and UNISTRA, Interreg IV Upper-Rhine Valley Program, project C25. J.C.B. is also grateful for the graduate and postgraduate scholarships from Ontario Graduate Scholarship Program (OGS) and Natural Sciences and Engineering Research Council of Canada (NSERC PDF program).

■ REFERENCES

(1) Byers, J. C.; Ballantyne, S.; Rodionov, K.; Mann, A.; Semenikhin, O. A. Mechanism of Recombination Losses in Bulk Heterojunction P3HT:PCBM Solar Cells Studied Using Intensity Modulated Photocurrent Spectroscopy. *ACS Appl. Mater. Interfaces* **2011**, *3*, 392−401.

(2) Street, R. A.; Cowan, S.; Heeger, A. J. Experimental Test for Geminate Recombination Applied to Organic Solar Cells. *Phys. Rev. B: Condens. Matter Mater. Phys.* **2010**, *82*, 121301.

(3) Street, R. A.; Schoendorf, M.; Roy, A.; Lee, J. H. Interface State Recombination in Organic Solar Cells. *Phys. Rev. B: Condens. Matter Mater. Phys.* **2010**, *81*, 205307.

(4) Jørgensen, M.; Norrman, K.; Gevorgyan, S. A.; Tromholt, T.; Andreasen, B.; Krebs, F. C. Stability of Polymer Solar Cells. *Adv. Mater.* **2012**, *24*, 580−612.

(5) Rösch, R.; Tanenbaum, D. M.; Jørgensen, M.; Seeland, M.; Bärenklau, M.; Hermenau, M.; Voroshazi, E.; Lloyd, M. T.; Galagan, Y.; Zimmermann, B.; Würfel, U.; Hösel, M.; Dam, H. F.; Gevorgyan, S. A.; Kudret, S.; Maes, W.; Lutsen, L.; Vanderzande, D.; Andriessen, R.; Teran-Escobar, G.; Lira-Cantu, M.; Rivaton, A.; Uzunoğlu, G. Y.; Germack, D.; Andreasen, B.; Madsen, M. V.; Norrman, K.; Hoppe, H.; Krebs, F. C. Investigation of the Degradation Mechanisms of a Variety of Organic Photovoltaic Devices by Combination of Imaging Techniques—the ISOS-3 Inter-Laboratory Collaboration. *Energy Environ. Sci.* **2012**, *5*, 6521−6540.

(6) Teran-Escobar, G.; Tanenbaum, D. M.; Voroshazi, E.; Hermenau, M.; Norrman, K.; Lloyd, M. T.; Galagan, Y.; Zimmermann, B.; Hösel, M.; Dam, H. F.; Jørgensen, M.; Gevorgyan, S.; Kudret, S.; Maes, W.; Lutsen, L.; Vanderzande, D.; Würfel, U.; Andriessen, R.; Rösch, R.; Hoppe, H.; Rivaton, A.; Uzunoğlu, G. Y.; Germack, D.; Andreasen, B.; Madsen, M. V.; Bundgaard, E.; Krebs, F. C.; Lira-Cantu, M. On the Stability of a Variety of Organic Photovoltaic Devices by IPCE and in Situ IPCE Analyses–the ISOS-3 Inter-Laboratory Collaboration. *Phys. Chem. Chem. Phys.* **2012**, *14*, 11824−11845.

(7) Norrman, K.; Krebs, F. C. Lifetimes of Organic Photovoltaics: Using TOF-SIMS and 18O2 Isotopic Labelling to Characterise Chemical Degradation Mechanisms. *Sol. Energy Mater. Sol. Cells* **2006**, *90*, 213−227.

(8) Norrman, K.; Larsen, N. B.; Krebs, F. C. Lifetimes of Organic Photovoltaics: Combining Chemical and Physical Characterisation Techniques to Study Degradation Mechanisms. *Sol. Energy Mater. Sol. Cells* **2006**, *90*, 2793−2814.

(9) Norrman, K.; Gevorgyan, S. A.; Krebs, F. C. Water-Induced Degradation of Polymer Solar Cells Studied by H2(18)O Labeling. *ACS Appl. Mater. Interfaces* **2009**, *1*, 102−112.

DOI: 10.1021/acsami.6b12345
ACS Appl. Mater. Interfaces XXXX, XXX, XXX−XXX

(10) Jørgensen, M.; Norrman, K.; Krebs, F. C. Stability/degradation of Polymer Solar Cells. *Sol. Energy Mater. Sol. Cells* **2008**, *92*, 686−714.
(11) Krebs, F. C.; Norrman, K. Analysis of the Failure Mechanism for a Stable Organic Photovoltaic during 10 000 H of Testing. *Prog. Photovoltaics* **2007**, *15*, 697−712.
(12) Petersen, M. H.; Gevorgyan, S. A.; Krebs, F. C. Thermocleavable Low Band Gap Polymers and Solar Cells Therefrom with Remarkable Stability toward Oxygen. *Macromolecules* **2008**, *41*, 8986−8994.
(13) Zimmermann, B.; Würfel, U.; Niggemann, M. Longterm Stability of Efficient Inverted P3HT:PCBM Solar Cells. *Sol. Energy Mater. Sol. Cells* **2009**, *93*, 491−496.
(14) Steim, R.; Kogler, F. R.; Brabec, C. J. Interface Materials for Organic Solar Cells. *J. Mater. Chem.* **2010**, *20*, 2499.
(15) Krebs, F. C. Encapsulation of Polymer Photovoltaic Prototypes. *Sol. Energy Mater. Sol. Cells* **2006**, *90*, 3633−3643.
(16) Seemann, A.; Sauermann, T.; Lungenschmied, C.; Armbruster, O.; Bauer, S.; Egelhaaf, H.-J.; Hauch, J. Reversible and Irreversible Degradation of Organic Solar Cell Performance by Oxygen. *Sol. Energy* **2011**, *85*, 1238−1249.
(17) Schafferhans, J.; Baumann, A.; Wagenpfahl, A.; Deibel, C.; Dyakonov, V. Oxygen Doping of P3HT:PCBM Blends: Influence on Trap States, Charge Carrier Mobility and Solar Cell Performance. *Org. Electron.* **2010**, *11*, 1693−1700.
(18) Manceau, M.; Rivaton, A.; Gardette, J.-L.; Guillerez, S.; Lemaître, N. Light-Induced Degradation of the P3HT-Based Solar Cells Active Layer. *Sol. Energy Mater. Sol. Cells* **2011**, *95*, 1315−1325.
(19) Kumar, M.; Dubey, A.; Reza, K. M.; Adhikari, N.; Qiao, Q.; Bommisetty, V. Origin of Photogenerated Carrier Recombination at the Metal-Active Layer Interface in Polymer Solar Cells. *Phys. Chem. Chem. Phys.* **2015**, *17*, 27690−27697.
(20) MacKenzie, R. C. I.; Balderrama, V. S.; Schmeisser, S.; Stoof, R.; Greedy, S.; Pallarès, J.; Marsal, L. F.; Chanaewa, A.; von Hauff, E. Loss Mechanisms in High Efficiency Polymer Solar Cells. *Adv. Energy Mater.* **2016**, *6*, 1501742.
(21) Shao, G.; Glaz, M. S.; Ma, F.; Ju, H.; Ginger, D. S. Intensity-Modulated Scanning Kelvin Probe Microscopy for Probing Recombination in Organic Photovoltaics. *ACS Nano* **2014**, *8*, 10799−10807.
(22) Set, Y. T.; Li, B.; Lim, F. J.; Birgersson, E.; Luther, J. Analytical Modeling of Intensity-Modulated Photovoltage Spectroscopic Responses of Organic Bulk-Heterojunction Solar Cells. *Appl. Phys. Lett.* **2015**, *107*, 173301.
(23) Pockett, A.; Eperon, G. E.; Peltola, T.; Snaith, H. J.; Walker, A.; Peter, L. M.; Cameron, P. J. Characterization of Planar Lead Halide Perovskite Solar Cells by Impedance Spectroscopy, Open-Circuit Photovoltage Decay, and Intensity-Modulated Photovoltage/Photocurrent Spectroscopy. *J. Phys. Chem. C* **2015**, *119*, 3456−3465.
(24) Set, Y. T.; Heinemann, M. D.; Birgersson, E.; Luther, J. On the Origin of the Quadrant I Semicircle in Intensity-Modulated Photocurrent Spectra of P3HT:PCBM Bulk Heterojunction Solar Cells: Evidence of Degradation-Related Trap-Assisted Recombination. *J. Phys. Chem. C* **2013**, *117*, 7993−8000.
(25) Gao, J.; Thomas, A. K.; Johnson, R.; Guo, H.; Grey, J. K. Spatially Resolving Ordered and Disordered Conformers and Photocurrent Generation in Intercalated Conjugated Polymer/Fullerene Blend Solar Cells. *Chem. Mater.* **2014**, *26*, 4395−4404.
(26) Gao, Y.; Wise, A. J.; Thomas, A. K.; Grey, J. K. Spectroscopic and Intensity Modulated Photocurrent Imaging of Polymer/Fullerene Solar Cells. *ACS Appl. Mater. Interfaces* **2016**, *8*, 285−293.
(27) Jouane, Y.; Colis, S.; Schmerber, G.; Kern, P.; Dinia, A.; Heiser, T.; Chapuis, Y.-A. Room Temperature ZnO Growth by Rf Magnetron Sputtering on Top of Photoactive P3HT: PCBM for Organic Solar Cells. *J. Mater. Chem.* **2011**, *21*, 1953.
(28) Chirvase, D.; Parisi, J.; Hummelen, J. C.; Dyakonov, V. Influence of Nanomorphology on the Photovoltaic Action of Polymer−fullerene Composites. *Nanotechnology* **2004**, *15*, 1317−1323.
(29) Li, J.; Peter, L. M. Surface Recombination at Semiconductor Electrodes. Part III. Steady-state and intensity modulated photocurrent response. *J. Electroanal. Chem. Interfacial Electrochem.* **1985**, *193*, 27−47.
(30) Li, J.; Peter, L. M. Surface Recombination at Semiconductor Electrodes. Part IV. Steady-state and intensity modulated photocurrents at n-GaAs electrodes. *J. Electroanal. Chem. Interfacial Electrochem.* **1986**, *199*, 1−26.
(31) Peter, L. M. Dynamic Aspects of Semiconductor Photoelectrochemistry. *Chem. Rev.* **1990**, *90*, 753−769.
(32) Rotenberg, Z. A.; Semenikhin, O. A. Intensity Modulated Photocurrents on an Anodically Oxidized Lead Electrode in Sulfuric Acid Solution. *J. Electroanal. Chem. Interfacial Electrochem.* **1991**, *316*, 165−174.
(33) Semenikhin, O. A.; Kazarinov, V. E.; Jiang, L.; Hashimoto, K.; Fujishima, A. Suppression of Surface Recombination on TiO_2 Anatase Photocatalysts in Aqueous Solutions Containing Alcohol. *Langmuir* **1999**, *15*, 3731−3737.
(34) DiCarmine, P. M.; Semenikhin, O. A. Intensity Modulated Photocurrent Spectroscopy (IMPS) of Solid-State Polybithiophene-Based Solar Cells. *Electrochim. Acta* **2008**, *53*, 3744−3754.
(35) Tremolet de Villers, B.; Tassone, C. J.; Tolbert, S. H.; Schwartz, B. J. Improving the Reproducibility of P3HT:PCBM Solar Cells by Controlling the PCBM/Cathode Interface. *J. Phys. Chem. C* **2009**, *113*, 18978−18982.
(36) Peter, L. M.; Wijayantha, K. G. U.; Tahir, A. A. Kinetics of Light-Driven Oxygen Evolution at α-Fe_2O_3 Electrodes. *Faraday Discuss.* **2012**, *155*, 309.

DOI: 10.1021/acsami.6b12345
ACS Appl. Mater. Interfaces XXXX, XXX, XXX−XXX